# Numerical simulations of the flows past two parallel square columns by MPS method



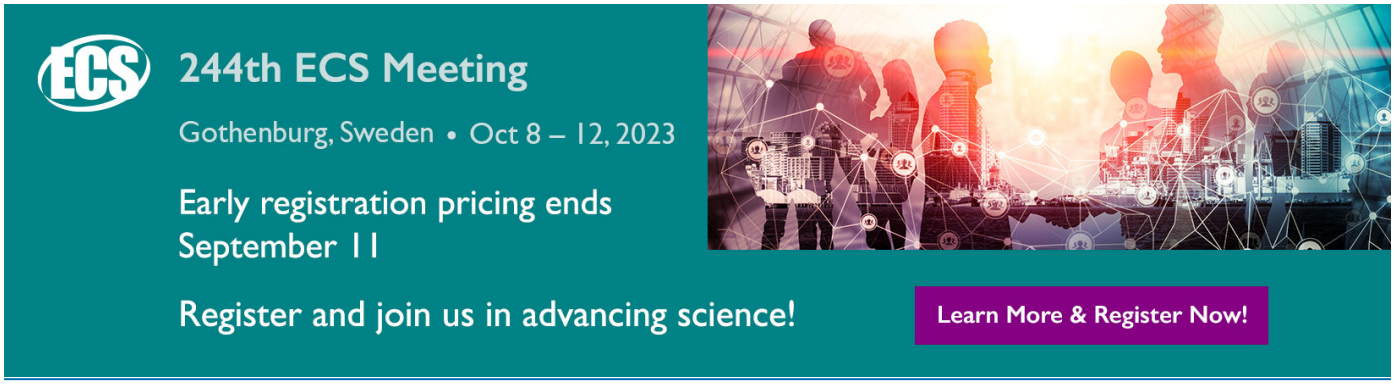

# Numerical simulations of the flows past two parallel square columns by MPS method

**Congyi Huang[1], Xiaolong Yang[2] and Decheng Wan[1]***

[1] Computational Marine Hydrodynamics Lab (CMHL), School of Naval Architecture, Ocean and Civil Engineering, Shanghai Jiao Tong University, Shanghai, China
[2] Offshore Oil Engineering Co. Ltd., Tianjin, China
*Corresponding Author: dcwan@sjtu.edu.cn

**Abstract**. The hydrodynamic interactions between an offshore platform and surrounding water mainly occurs in way of the pile legs, and the flow past the pile legs can be simplified to the flow past the columns. This is the reason why it is of great significance to simulate the flow around multiple columns with accuracy. In this paper, based on a mesh-less method, Moving Particle Semi-implicit (MPS) method, the MLParticle-SJTU solver is used to simulate the flow past two parallel square columns. Firstly, the reliability and accuracy of the solver is verified by simulating the Poiseuille flow, in which the no-slip boundary condition is applied. Then, the flow past two parallel square columns with different spacing between the two columns is simulated when the Reynold number is 40. The influence of spacing on flow pattern, force on columns and the vortex shedding frequency is analyzed. It is found that when the spacing is relatively small, small vortices will be attached to the surface of the columns. As the spacing ratio increases, periodic shedding of vortices will occur.

## 1. Introduction

In the field of naval architecture and ocean engineering, simulating the motion of offshore platforms exactly is a very important problem. The interaction between the platforms and the fluid mainly happens at platform's pile legs, which can be simplified as the flow past columns. The flow around a cylinder is a very classic and representative problem, and many researchers have conducted relevant research and discussion on this issue. Although the calculation model of this problem is very simple, there are many kinds of complex flow phenomena in this process, such as flow separation, vortex generation and shedding. Therefore, it is of great significance to simulate this process accurately. When simulating the flow around the columns of an offshore platform, each pile leg cannot be simply regarded as an independent column. The interaction among the columns is very important and should be considered. Therefore, the study of the flow around two columns has great engineering significance and academic value.

In recent years, with the rapid development of computer, CFD method has been used in simulating engineering problems more and more widely. And many scholars have studied the flow around a cylinder through numerical simulations. According to whether the computational domain needs to be divided into meshes, CFD methods can be divided into mesh-based methods and meshless particle methods. Different from traditional mesh-based method, the meshless particle methods use discrete particles to represent the computational domain. There is no fixed topological relationship between each particle, and each carries physical quantities such as mass, pressure and velocity. The traditional mesh

methods often encounter the problem of mesh fragmentation when dealing with the problems with large deformation characteristics of free surface. However, meshless particle methods naturally overcome this problem due to their Lagrangian property. Therefore, the meshless methods have received widespread attention and application in recent years. In 2009, Yildiz et al. [1] proposed a multi-layer boundary particle approach to deal with boundaries, which solved the problem that the particle method could not deal with curved boundaries correctly. For the first time, the SPH method was used to simulate the flow around a cylinder with Reynolds number 50. In 2015, Shibata et al. [2] simulated the flow around a cylinder with Reynolds number of 100 and 200 using MPS method, and successfully simulated the Karman vortex street behind the cylinder and square cylinder. Zhou et al. [3] used direct numerical simulation methods to analyze the changes in turbulence intensity and energy of the flow field around parallel columns. Jamshed et al. [4] conducted a numerical simulation on the flow around two parallel porous square columns. Based on the analysis of the influence of Reynolds number and spacing ratio, the influence of permeability on the flow is further analyzed. Sahu et al. [5] investigated the turbulent flow properties experimentally in the vicinity of two side-by-side circular cylinders, along with the influence of the third cylinder of the same dimension placed in the upstream and successively in the downstream forming an equilateral triangle.

In this paper, the methods and boundary conditions used in this article is briefly introduced firstly. After that, the accuracy of the method and the stability of the solver is verified by simulating the Poiseuille flow. Finally, the flow past two parallel columns is simulated and the influence of spacing on the flow pattern is analyzed. The present work contributes to better optimization of platform design in engineering application.

## 2. Numerical method

The MPS method is a meshless particle method based on the Lagrange representation. The computational domain is represented by discrete particles. These particles are not connected by grids or nodes, but carry physical quantities such as mass, velocity and acceleration separately. The flow field is controlled by establishing the governing equation.

### *2.1. Governing equations*

The governing equations include the continuity equation and the momentum equation. The governing equation for viscous incompressible fluid can be written as:

$$\frac{1}{\rho}\frac{D\rho}{Dt} = -\nabla \cdot \boldsymbol{V} = 0 \tag{1}$$

$$\frac{D\boldsymbol{V}}{Dt} = -\frac{1}{\rho}\nabla P + \nu\nabla^2\boldsymbol{V} + \boldsymbol{g} \tag{2}$$

where $\rho$ is fluid density, $\boldsymbol{V}$ is velocity vector, $P$ presents pressure, $\nu$ is kinematic viscosity, $\boldsymbol{g}$ is gravitational acceleration vector, $t$ indicates time.

### *2.2. Discretization of the governing equations*

In the MPS method, the computational domain is composed of discrete particles. Therefore, the governing equations need to be discretized.

*2.2.1. Kernel function* In the MPS method, the interaction between particles is realized by the kernel function, which can be written as:

$$W(r) = \begin{cases} \dfrac{r_e}{0.85r + 0.15r_e} - 1 & 0 \le r < r_e \\ 0 & r_e \le r \end{cases} \tag{3}$$

where $r = |\boldsymbol{r}_j - \boldsymbol{r}_i|$ represents the distance between particle *i* and *j*, $r_e$ is the influence radius.

*2.2.2. Density of the particle number.* The particle number density is the sum of kernel functions of all the particles within the influence radius, which can be written as:

$$\langle n \rangle_i = \sum_{j \neq i} W\left(|\boldsymbol{r}_j - \boldsymbol{r}_i|\right) \tag{4}$$

for incompressible fluid, the particle number density remains constant.

*2.2.3. Gradient model.* The gradient model is used to discretize the pressure gradient in the governing equation. The expression is:

$$\langle \nabla P \rangle_i = \frac{D}{n^0} \sum_{j \neq i} \frac{P_j + P_i}{|\boldsymbol{r}_j - \boldsymbol{r}_i|^2} (\boldsymbol{r}_j - \boldsymbol{r}_i) W(|\boldsymbol{r}_j - \boldsymbol{r}_i|) \tag{5}$$

where *D* represents the dimension and  represents the initial particle number density.

*2.2.4. Divergence model.* Similar to the gradient model, the divergence model is used to discretize the velocity divergence in the governing equation. The expression is:

$$\langle \nabla \cdot \boldsymbol{V} \rangle_i = \frac{D}{n^0} \sum_{j \neq i} \frac{(\boldsymbol{V}_j - \boldsymbol{V}_i) \cdot (\boldsymbol{r}_j - \boldsymbol{r}_i)}{|\boldsymbol{r}_j - \boldsymbol{r}_i|^2} W(|\boldsymbol{r}_j - \boldsymbol{r}_i|) \tag{6}$$

*2.2.5. Laplacian model.* Laplacian model is used to discretize the second derivative in the governing equation, which can be expressed as:

$$\langle \nabla^2 \phi \rangle_i = \frac{2D}{n^0 \lambda} \sum_{j \neq i} (\phi_j - \phi_i) W(|\boldsymbol{r}_j - \boldsymbol{r}_i|) \tag{7}$$

where $\lambda$ represents the correction of the error introduced by the kernel function, and it can be written as:

$$\lambda = \frac{\sum_{j \neq i} W\left(|\boldsymbol{r}_j - \boldsymbol{r}_i|\right) |\boldsymbol{r}_j - \boldsymbol{r}_i|^2}{\sum_{j \neq i} W\left(|\boldsymbol{r}_j - \boldsymbol{r}_i|\right)} \tag{8}$$

*2.3. Pressure Poisson equation*

In the MPS method, the Poisson equation is used to solve the particle pressure. The incompressibility of fluid is determined by divergence-free condition and constant particle number density condition. The Poisson equation adopted in this paper is as follows:

$$\langle \nabla^2 P^{k+1} \rangle_i = (1-\gamma) \frac{\rho}{\Delta t} \nabla \cdot \boldsymbol{V}_i^* - \gamma \frac{\rho}{\Delta t^2} \frac{< n^k >_i - n^0}{n^0} \tag{9}$$

where superscripts k and k+1 represent k and k+1 time steps.  is a variable parameter, representing the proportion of particle number density in the source term of Poisson equation. In the numerical simulation in this paper,  takes 0.01. (Tanaka and Masunaga[6], Lee et al, [7])

*2.4. Detection of free surface particles*

When solving the Poisson's pressure equation, it is very important to determine whether a particle is located on a free surface. The number density of particles can be used to determine whether a particle is on a free surface in MPS method. When $\langle n \rangle_i < 0.8 n^0$, the particle is considered to be on a free surface. When $\langle n \rangle_i > 0.97 n^0$, the particles are thought to be inside the fluid. For particles with particle number density between 0.8 and 0.97, it's difficult to tell whether the particle is on the free surface or inside the

fluid. Khayyer and Gotoh [8] first proposed the criterion which simply based on the fact that for a free-surface particle, the distribution of neighboring particles is asymmetric. In this paper, the vector function $\boldsymbol{F}$ presented by Zhang et al. [9] is introduced, as follows:

$$< \boldsymbol{F} >_i = \frac{D}{n^0} \sum_{j \neq i} \frac{(\boldsymbol{r}_i - \boldsymbol{r}_j)}{|\boldsymbol{r}_i - \boldsymbol{r}_j|} W(|\boldsymbol{r}_i - \boldsymbol{r}_j|) \tag{10}$$

If $\langle |\boldsymbol{F}| \rangle_i > 0.9 |\boldsymbol{F}|^0$, the particle i will be considered to be on a free surface. $|\boldsymbol{F}|^0$ stands for $|\boldsymbol{F}|$ at the initial time of the free surface particle.

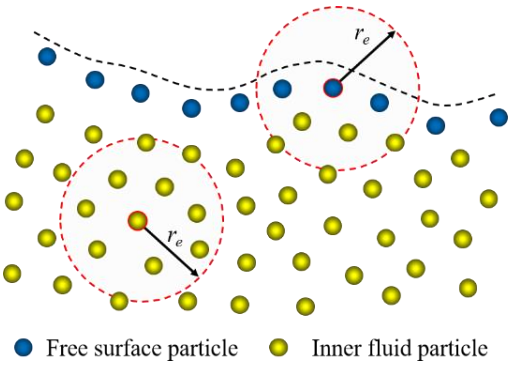


**Figure 1.** Schematic diagram of free surface particle judgment.

## 3. Numerical simulation

### *3.1. Reliability verification*

In this section, the reliability of the MLParticle-SJTU solver used in this article is verified by simulating the Poiseuille flow. The theoretical velocity distribution of Poiseuille flow is given in the following equation.

$$u = \frac{6Q}{h^3}(y^2 - hy) \tag{11}$$

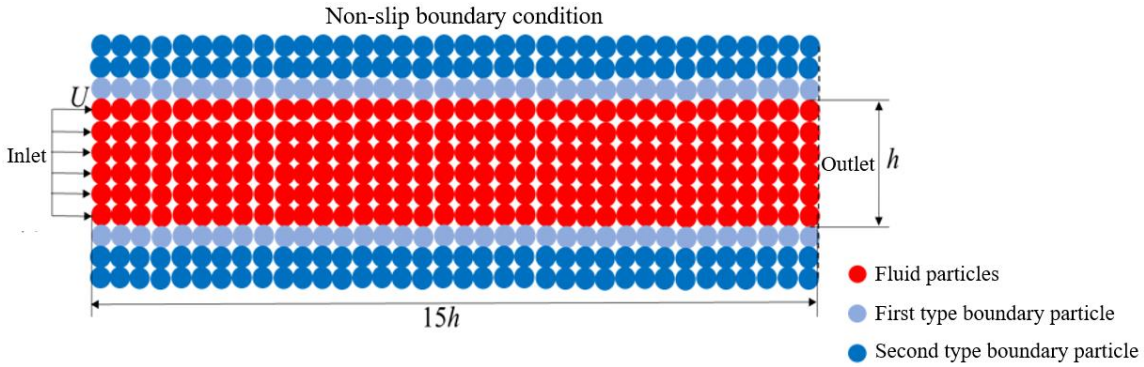


**Figure 2.** Schematic diagram of computational domain.

The computational domain is shown in Figure 2. It can be seen that the boundary conditions used in this paper is composed of multiple layers of particles, one layer of first type boundary particles and two layers of second type boundary particles. The first type of boundary particles is used to provide repulsive

force to fluid particles, while the second type of boundary particles is used to ensure the integrity of the fluid particle support domain. The first type boundary particles participate in solving the pressure Poisson equation, while the pressure of the second type boundary particles is obtained by interpolation between fluid particles and the first type boundary particles. In addition, non-slip boundary conditions need to be applied when simulating Poiseuille flow. In this paper, the method of moving virtual mirror particles proposed by Lee et al. [7] is used, as shown in Figure 3.

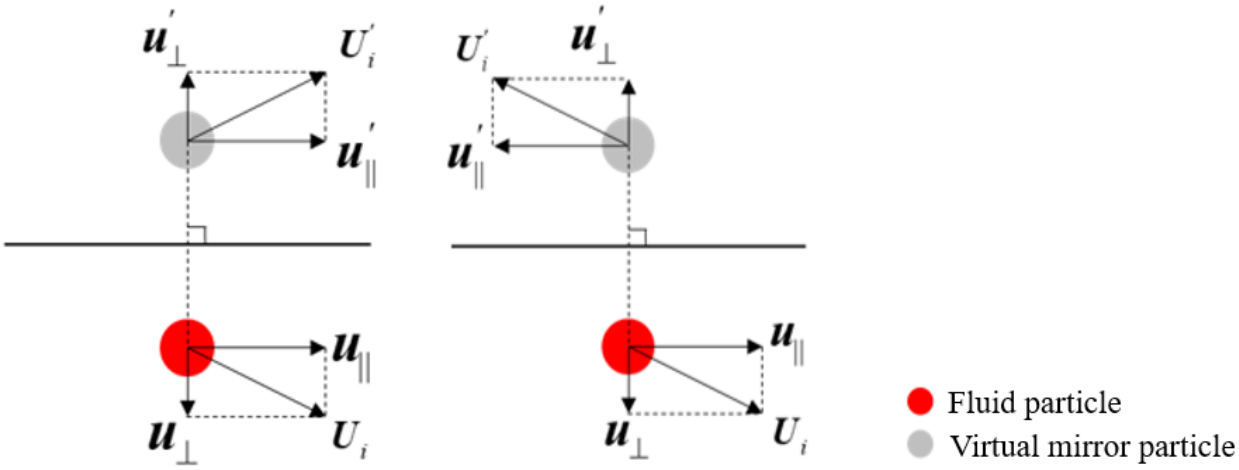


**Figure 3.** Schematic diagram of slip and non-slip boundary conditions.

In figure 3, $\boldsymbol{U}_i$, $\boldsymbol{u}_\perp$ and $\boldsymbol{u}_\parallel$ represent the velocity, vertical and parallel components of fluid particles respectively. $\boldsymbol{U}_i^{'}$, $\boldsymbol{u}_\perp^{'}$ and $\boldsymbol{u}_\parallel^{'}$ represent the velocity and components of virtual mirror particles corresponding to fluid particles. When calculating the viscous force at each time step, virtual mirror particles are generated on the outer side of the boundary. The virtual mirror particles and fluid particles are axisymmetric about the boundary. When the boundary is stationary, under the non-slip boundary condition, the vertical and parallel velocity components of virtual mirror particles are opposite to those of fluid particles. Under slip boundary condition, the vertical velocity component of virtual mirror particles is opposite to that of fluid particles, while the parallel velocity component is the same as that of fluid particles.

The calculation model is shown as figure 2, the diameter $h$ of the pipeline is 0.2m and the length of the pipeline is 15$h$, which is an enough distance for the flow to fully develop. The Poiseuille flow is simulated at Reynolds number is 4, and the velocity distribution is shown in Figure 4. It can be seen that the flow velocity in the pipe distributs evenly, showing the characteristics of high velocity near the central line and low velocity near the pipe wall, which conforms to physical characteristics and proves the validity and rationality of the boundary conditions used in this article.

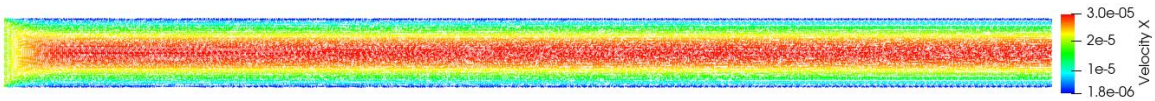


**Figure 4.** Velocity distribution of the Poiseuille flow.

Next, the velocity profile at x=10h cross-section at different times is drawn as shown in figure 5. It can be seen that when Ut/h=0.5, the flow has developed to a stable state, and the velocity profile almost coincides with the analytical solution, which can verify the correctness of the proposed method and the accuracy and stability of the MLParticle-SJTU solver.

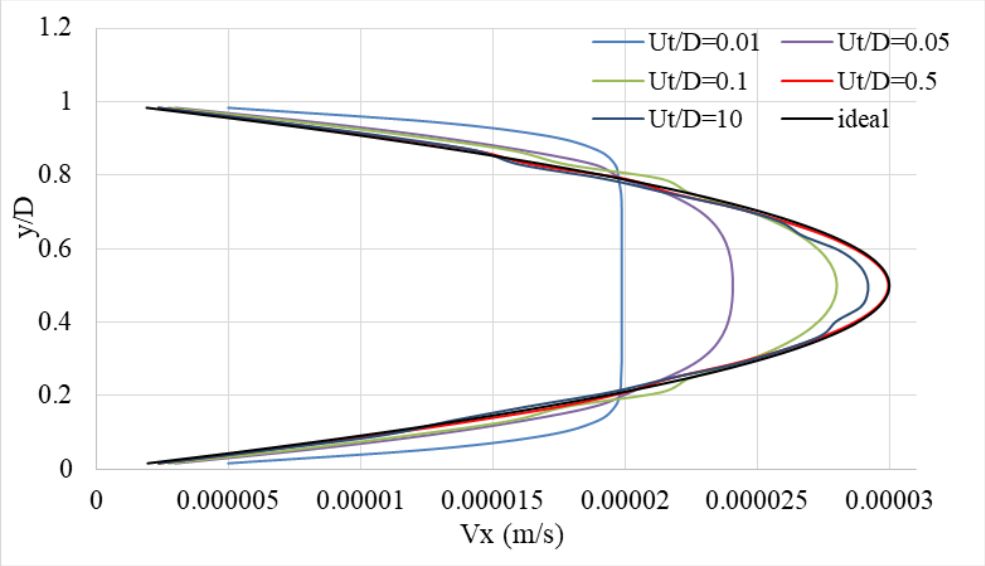


**Figure 5.** Velocity profiles at different times at x=10h.

*3.2. Numerical Simulation of the flow past two parallel square columns*

Since the accuracy and validity of the numerical method used in this paper is confirmed in the previous subsections, the flow past two parallel square columns will be simulated in this part. The Reynolds number is set as 40, and the influence of the spacing between square cylinders on the vortex shedding frequency, lift drag on the columns is analysed.

*3.2.1. Calculation domain selection and boundary condition setting*

The schematic diagram of the computational domain is shown in Figure 6. The side length D of the square column is 0.1 m, H is the distance between the two square columns, and the spacing ratio is set as H/D=1.2-5.0. The initial particle spacing is set to D/ Δ x=20. Schematic diagrams of the velocity distribution obtained from the simulation with different spacing ratios at Ut/D=200 are shown in Figure 7. In the following parts, the fluid is assumed to be viscous and incompressible, and the friction between the fluid and the square column is not considered

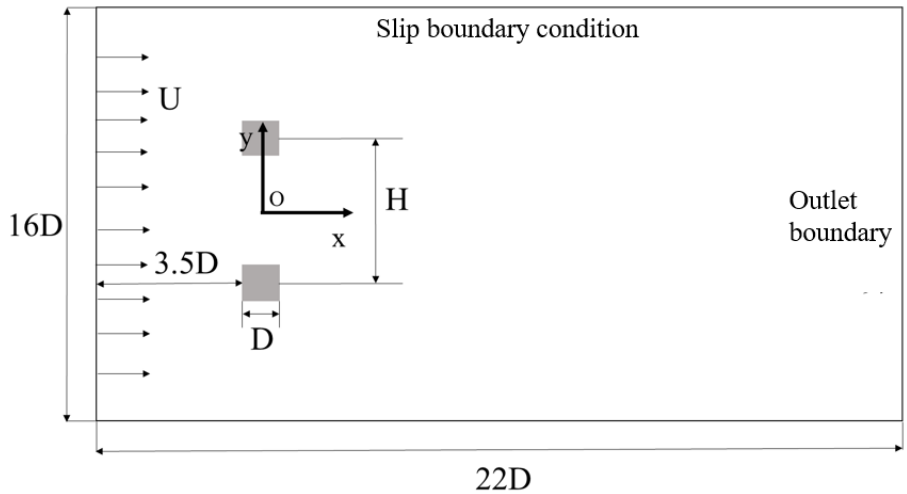


**Figure 6.** Schematic diagram of calculation domain for parallel two column examples.

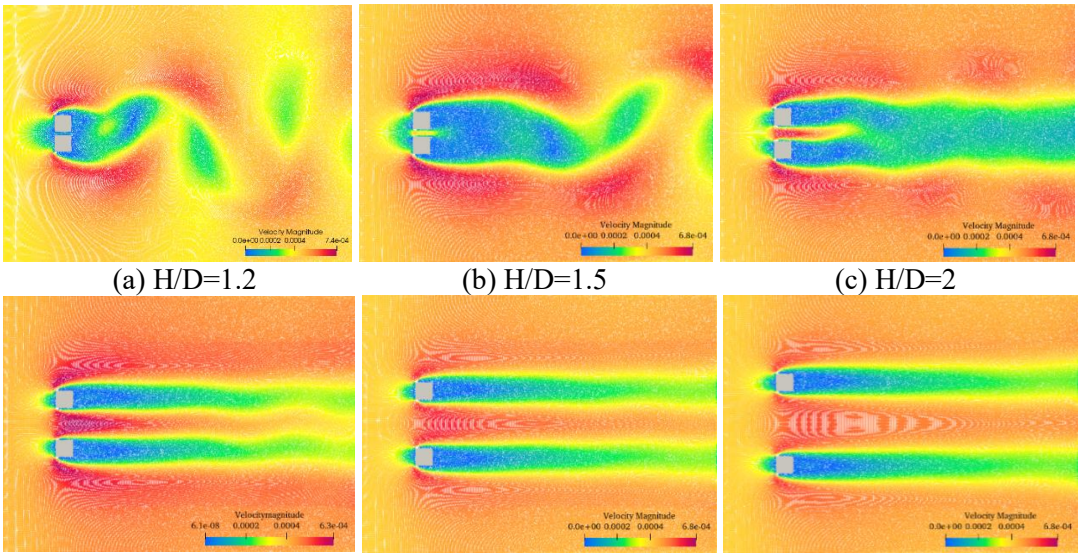

(a) H/D=1.2 (b) H/D=1.5 (c) H/D=2

(d) H/D=3 (e) H/D=4 (f) H/D=5

**Figure 7.** Velocity distribution at different spacing ratios at Ut/D=200.

From Figure 7, it can be seen that the velocity distribution obtained by MPS method is uniform and very stable. When H/D=1.2 and 1.5, the wake behind the two square columns is connected to form a large wake region and oscillates periodically, but the length of the wake is significantly shorter under H/D=1.2 than H/D=1.5. When H/D=2, the wake behind the square columns is separated near the trailing edge of the square column, but at a certain distance from the square column, the two wakes merge. When H/D=3, the two wakes have completely separated, but as can be seen from the distant wakes, mutual interference still exists. When H/D=4 and 5, the wake in the computational domain is almost straight and there is almost no obvious mutual interference.

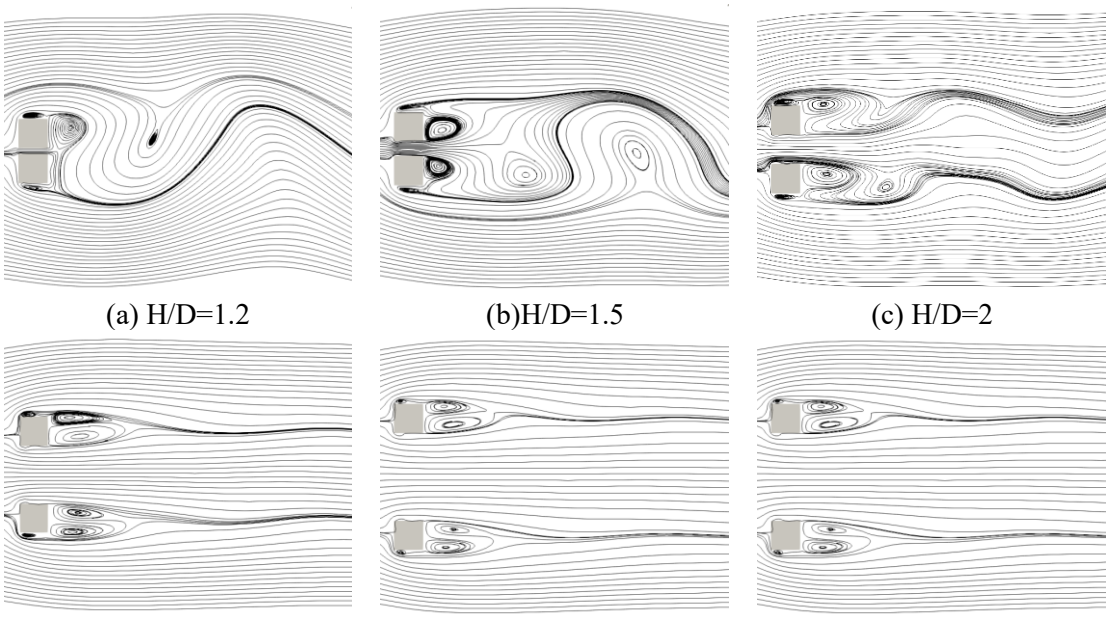

(a) H/D=1.2 (b)H/D=1.5 (c) H/D=2

(d)H/D=3 (e) H/D=4 (f)H/D=5

**Figure 8.** Streamlines around two parallel square columns at different H/D with Re=40.

To further investigate the formation and shedding of the vortex near the square column, the streamline diagram is drawn, as shown in Figure 8. It can be seen from that when the spacing ratio is 1.2, 1.5, and 2, vortices detach behind the square column, and small vortices are generated near the sharp corners of the column. As the spacing ratio increases, the mutual influence between the square columns weakens. Under the conditions of H/D=3, 4, and 5, the vortex shedding phenomenon behind the square column disappears and returns to a steady flow state. However, the wake behind the square column exhibits obvious asymmetric characteristics.

Figure 9 shows the average velocity profile curves at different positions under different spacing ratios. Under the condition of H/D=1.2, the x/D=0 curve exhibits negative values near y/D=±1.1. Based on the analysis in Figure 8 (a), this may be due to the formation of small eddies here. At the same time, it can be seen that the velocity between the two columns is very small, so the flow past the parallel two columns can be approximated as the flow around a single square column under this spacing ratio. The velocity profiles of each section behind the columns also exhibit a "V" shape, and tend to flatten along the flow direction, which is consistent with the results shown in Figures 7 and 8.

Under the condition of H/D=1.5, there are still small vortices on the outer surfaces of the two square columns, so the x/D=0 curve shows a negative value at y/D=± 1.25. The flow velocity between the two square columns is much higher than that under the H/D=1.2 condition. The x/D=2 curve shows a region below zero behind both columns, possibly because that two stable vortices is formed and attached to each column at this time. At x/D=5, the velocity curve has only a minimum value, which is less than zero at y=0. The reason for this phenomenon may be that at the position where y=0, periodically shed vortices form a reflux zone.

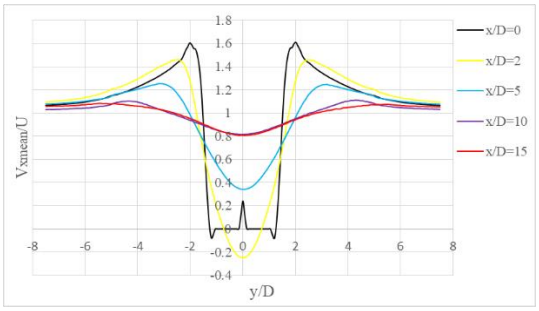


(a) H/D=1.2

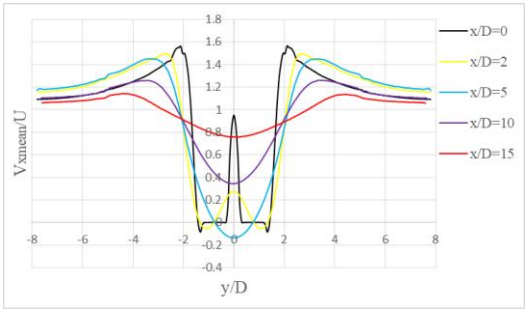


(b) H/D=1.5

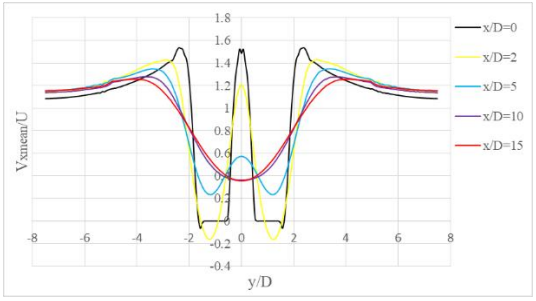


(c) H/D=2

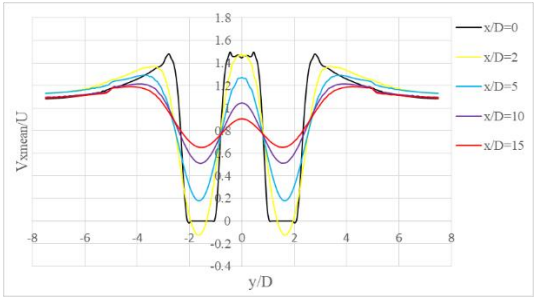


(d) H/D=3

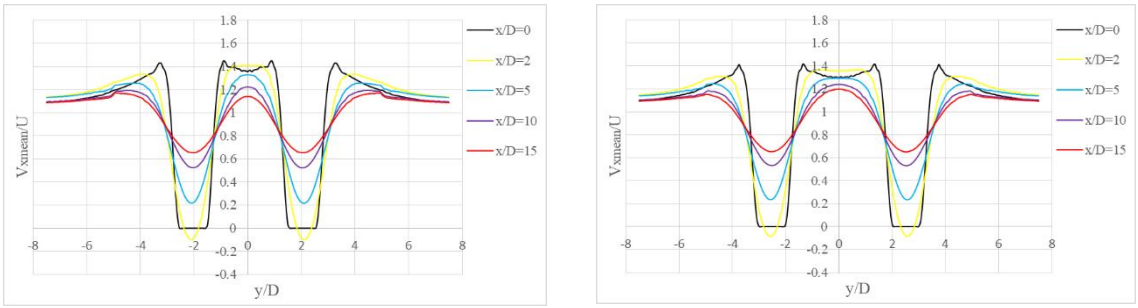


(e) H/D=4 (f) H/D=5

**Figure 9.** Average velocity profile curves at different H/D with Re=40.

When H/D=2, it can be seen from the x/D=0 curve that small vortices still exist on the columns, and the flow velocity between the two square columns is higher than the results mentioned earlier. The x/D=2 curve still has two minimum values less than zero like under H/D=1.5 condition, but the formation reasons for these two cases may be different. At this time, there is no stable attached vortex behind the column, and the less than zero average velocity may be formed by the periodic shedding vortices after the two square columns. The x/D=5 curve still has two minimum values, but at this point, the minimum value is higher than zero. At x/D=10, the wake merges and only one minimum value appears at the central line between the two columns.

Under H/D=3, 4, and 5 conditions, there are two minimum values for sections with x/D≥2, because the wake behind the two columns does not merge. However, due to the mutual influence between the square columns, it can be seen that the minimum values are not located on the central line of the square column, but slightly off central line.

**Table1.** Peak average velocity at x/D=0.

| H/D | 1.2 | 1.5 | 2 | 3 | 4 | 5 |
|---|---|---|---|---|---|---|
| $V_{meanmax}/U$ | 1.604 | 1.562 | 1.535 | 1.480 | 1.429 | 1.411 |

Table 1 shows the peak value of the average velocity curve of the flow around the two columns at x=0 under different spacing ratios. It can be seen that with the increase of spacing ratio H/D, the velocity peak decrease. As the Reynolds number is 40, it is close to the critical Reynolds number when the flow changes from steady to unsteady state. The fluid flows past the column, leading to an increase velocity on both sides, which may be one of the reasons for the periodic vortex shedding phenomenon when the spacing ratio H/D≤2.

## 4. Conclusions

The flow past two parallel square columns is simulated based on MPS method in this particle. Firstly, the stability of the MLParticle-SJTU solver used in this paper is verified by simulating Poiseuille flow at Reynolds number 4. Next, the flow around two parallel columns is simulated. By analyzing the velocity distribution under different spacing ratios at Ut/D=200, it is found that when the spacing ratio H/D<2, the interaction between the two square columns is very obvious. The wake behind the two columns is very similar to that of a single square column, presenting a large oscillating wake. However, as the spacing ratio increases, the wake behind the square column becomes longer. After H/D>3, the wake behind the two square columns are already independent of each other, but mutual interference can also be observed.

Then, the vortices formation and shedding in the flow around the square column are further analyzed by streamlines and average velocity profiles at different sections. The results indicate that when H/D<2, small vortices generates at the sharp corners of the two columns, so the average velocity there is less than 0. At x/D=2, except for only one minimum value under the H/D=1.2 condition, there are two minimum values less than 0 in the other five conditions. It may be due to the formation of stable vortices attached to the square column here, or it may be due to the formation of stable shedding vortices here. For H/D=3, 4, and 5, the wakes of the two square columns are independent of each other, but there is still mutual influence. The streamline diagrams of the two square columns show asymmetric display, and the minimum values of the velocity profile do not appear on the central line of the square column, but appear slightly off the central line.

In this paper the two-dimensional square column winding process is simulated. In the future, the work will be extended to three dimensions, and the flow past multi-columns will be simulated.

**Acknowledgements**
This work was supported by the National Natural Science Foundation of China (52131102), and the National Key Research and Development Program of China (2019YFB1704200), to which the authors are most grateful.

**References**
[1] Yildiz M, Rook R A and Suleman A 2009 SPH with the multiple boundary tangent method *Int. J. Numer. Methods Eng.***77(10)** 1416-38.
[2] Shibata K, Koshizuka S, Murotani K, Sakai M and Masaie I 2015 Boundary conditions for simulating Karman vortices using the MPS Method *J. Adv. Simul. Sci. Eng.***2(2)** 235-54.
[3] Zhou Y, Nagata K, Sakai Y. Watanabe T and Hayase T 2020 Energy transfer in turbulent flows behind two side-by-side square cylinders *J. Fluid Mech.* **903(A4)** 1-31.
[4] Jamshed S, Dhiman A 2021 Channel-Confined Wake Structure Interactions Between Two Permeable Side-by-Side Bars of a Square Cross-Section *J. Fluid Mech.* **143** 091301.
[5] Sahu C, Eldho T I, Mazumder B S 2023 Experimental Study of Flow Hydrodynamics Around Circular Cylinder Arrangements Using Particle Image Velocimetry *J. Fluids Eng.-Trans. ASME* **145(1)** 011302.
[6] Tanaka M and Masunaga T 2010 Stabilization and Smoothing of Pressure in MPS Method by Quasi-Compressibility *J. Comput. Phys.* **229(11)** 4279–90.
[7] Lee B H, Park J C, Kim M H and Hwang S C 2011 Step-by-step improvement of mps method in simulating violent free-surface motions and impact-loads. *Comput. Meth. Appl. Mech. Eng.* **200(9-12)** 1113-25.
[8] Khayyer A, Gotoh H and Shao S 2009 Enhanced predictions of wave impact pressure by improved incompressible SPH methods, *Appl. Ocean Res.* **31(2)** 111-31.
[9] Zhang Y, Wan D 2012 Apply MPS method to simulate liquid sloshing in LNG tank. *Proc. of the 22nd Int. Offshore and Polar Eng. Conf.* (Rhodes, Greece) 381-91.
[10] Koshizuka S, Nobe A and Oka Y 1998 Numerical Analysis of Breaking Waves Using the Moving Particle Semi-implicit Method *Int. J. for Numer. Methods Fluids* **26(7)** 751-69.